Cancer Nanotechnology

RESEARCH Open Access

Dual-sensitive and highly biocompatible O-carboxymethyl chitosan nanodroplets for prostate tumor ultrasonic imaging and treatment

Dong Meng, Lu Guo, Dandan Shi, Xiao Sun, Mengmeng Shang, Shan Xiao, Xiaoying Zhou, Yading Zhao, Xiaoxuan Wang and Jie Li*

*Correspondence:
jieli301@163.com

Department of Ultrasound, Qilu Hospital of Shandong University, West Wenhua Road, Jinan, Shandong, China

Abstract

Nanosized drug delivery systems have rapidly emerged as a promising approach to tumor therapy, which still have many challenges in clinical application. In this study, doxorubicin-loaded O-carboxymethyl chitosan/perfluorohexane nanodroplets (O-CS-DOX NDs) were synthesized and functionally tested as an effective drug delivery system in vitro and in vivo. O-CS-DOX NDs with small size (159.6 nm) and good doxorubicin encapsuling ability showed pH- and ultrasound-dependent drug release profile and satisfying ultrasound imaging performance. With high biocompatibility and biosafety, these nanodroplets could accumulate in the tumor sites and exhibit high efficiency in inhibiting tumor growth with ultrasound irradiation. These stable, safe and smart O-CS-DOX NDs showed promising potential as a smart dual-responsive bomb for tumor ultrasonic imaging and treatment.

Keywords: O-carboxymethyl chitosan, Nanodroplets, pH-sensitive, High biocompatibility, Ultrasound-sensitive, Ultrasound imaging, Ultrasound-aided tumor therapy

Introduction

With great advances in cancer-targeted nanotechnology, nanosized drug delivery systems have rapidly emerged as a promising therapeutic approach to enhance the anticancer efficiency, reduce the multidrug resistance, and minimize drug-related side effects of chemotherapeutic drugs (Meel et al. 2019; Golombek et al. 2018; Chang et al. 2016; Kelly et al. 2014; Markman et al. 2013). In recent years, a wide variety of nanoparticles-based drug delivery systems have been developed, with some being employed in clinical diagnosis and therapy (Kanamala et al. 2016; Chen et al. 2018). However, current clinical used nanomedicines had failed to achieve considerable improvement in therapeutic efficacy, mostly due to limited delivery efficiency (Shi et al. 2017). Therefore, it is still challenging to further improve the

therapeutic efficacy of the carriers (Bae and Park 2011; Wang et al. 2020; Denison and Bae 2012; Rosenblum et al. 2018; Fisher et al. 2013). Recent studies are focusing on the rational design of the "smart stimulus-responsive nanoparticles" that can achieve a more specific and more effective delivery when exposed to tumor microenvironmental stimuli in vivo such as pH, enzyme, temperature, and magnetic field (Movahedi et al. 2015; Yusa 2017). Among all these, pH-sensitive nanoparticles were widely studied, which is also a hot topic, because of the significant pH difference between the normal physiological circulation and the tumor extracellular environment (Thakkar et al. 2019; Liu et al. 2014a). Over the last decade, numerous pH-sensitive nanoparticles were prepared successfully and proved to be the more effective and specific drug carriers in vitro and in vivo experiments (Li et al. 2015; Tian et al. 2014; Wang et al. 2014; Liu et al. 2014b; Yao et al. 2015; Wei et al. 2019; Zhao et al. 2017; Sonawane et al. 2017; Long et al. 2020; Han et al. 2021). Unexpectedly, their clinical translation suffered from operational complexity, nanoparticle toxicity and high expenses (Shen et al. 2018; Ma et al. 2020).

Compared with different nanoparticles developed in previous studies, we reported on a pH-sensitive charge-conversional and ultrasound-responsive nanodroplets-based drug delivery system in our previous study (Meng et al. 2019). With simple mild process of manufacture, these doxorubicin-loaded nanodroplets had great stability, superior ultrasound imaging ability and excellent targeting ability. More importantly, thanks to O-carboxymethyl chitosan material, these nanodroplets are better on pH-responsive, biocompatibility and enhanced antitumor effect, compared with previously reported nanoparticles. Diagnostic ultrasound imaging techniques and therapeutic capabilities were integrated into one single agent to achieve specific and individualized imaging diagnosis and drug therapy. Compared with CT/MRI imaging, ultrasound imaging is a common non-invasive, cost-effective, and well-controlled technique with its unique advantages of excellent penetration capability and real-time imaging and is allowed for safe clinical application (Lee et al. 2016; Chong et al. 2018). The PFH-based nanodroplets enhanced contrast ultrasound imaging and release the encapsulated drug at certain tumor tissues, after phrase-transformation process due to the "acoustic droplet vaporization (ADV)"effect of ultrasound irradiation (Yang et al. 2019). However, all these advantages of the nanodroplets in our previous study were shown only in vitro, and numerous nanomedicines had failed to achieve considerable improvement in vivo and clinical trials due to complex tumor microenvironment. Therefore, further investigation in vivo will be needed to explore the feasibility of these nanodroplets as a molecular imaging and treatment agent.

Herein, we pushed this O-CS- and PFH-based nanodroplets further toward in vivo cancer imaging and therapy. We expect that all the advantages of these vectors would be maintained with high biocompatibility in vivo. First, we improved the method for preparation of the previous doxorubicin-loaded O-CS nanodroplets (O-CS-DOX NDs) using another different safer emulsion method and reevaluate its characteristics as drug delivery system. Second, the ultrasound imaging ability and biocompatibility of O-CS-DOX NDs in PC-3 tumor-bearing mice were analyzed. Finally, tumor accumulation and antitumor efficiency were carefully examined.

Materials and methods

Chemicals

O-carboxymethyl chitosan (O-CS, MW 100–300 KD, degree of deacetylation 90%, degree of carboxymethylation 95%) was supplied by Santa Cruz Biotechnology (Dallas, USA). Chitosan (CS, MW 100–300 KD, degree of deacetylation 90%), Tween 20, lecithin and doxorubicin were purchased from Solarbio Sciences and Technology (Beijing, China). Perfluorohexane (PFH) was supplied by Macklin Biochemical (Shanghai, China). Deionized or distilled water was used in all experiments. All other chemicals and solvents were obtained commercially as analytical-grade reagents.

Preparation of doxorubicin-loaded nanodroplets

Both doxorubicin-loaded O-carboxymethyl chitosan nanodroplets (O-CS-DOX NDs) and doxorubicin-loaded chitosan nanodroplets (CS-DOX NDs) were prepared via nano-emulsification process using an ultrasonic crusher (VCX150, SONICS&MATERIALS, Inc., USA). Preliminary experiments were carried out to choose the optimal sonicating power. Briefly, a fixed-ratio mixture of PFH, Tween 20 (surfactant), lecithin (co-surfactant) and doxorubicin were sonicated in deionized water for 2 min at 150 W (10 s of operation and 10 s of rest in turn) under ice bath conditions. Then, O-CS (0.15% w/v) or CS (0.15% w/v in 1% v/v acetic acid, pH 5) was added dropwise to the emulsion while sonicating at 120 W for 1 min (10 s of operation and 10 s of rest in turn). The suspension was centrifuged at 500 rpm for 3 min. The lower layer was collected and ultra-centrifuged at 12,000 rpm for 5 min to separate the free doxorubicin from doxorubicin-loaded nanodroplets. The purified nanodroplets were resuspended in sterile PBS and stored at 4 ℃ for further use. All the experiments were carried out in dark place or with tinfoil to prevent fluorescence quenching.

Characterization of O-CS-DOX NDs

The morphology and structure of O-CS-DOX NDs were observed using scanning electron microscope, (SEM), (EVOMA 10, Zeiss, Germany) and transmission electron microscope, (TEM), (JEM-1011; JEOL, Japan). Samples were prepared by placing one drop of the solution on a 400-mesh carbon-coated copper grid and drying at room temperature. The shape was also observed with fluorescence microscopy. The average size distribution, polydispersity index and surface zeta potential of the nanodroplets were measured with Delsa Nano C Particle Size and Zeta Potential Analyzer (Beckman Coulter, USA). Each sample was analyzed in triplicate.

Entrapment efficiency and loading efficiency of O-CS-DOX NDs

Supernatants recovered from ultra-centrifuging of O-CS-DOX NDs mentioned above were decanted. Doxorubicin content in the supernatant was analyzed by a Microplate Spectrophotometer (UV-2450) at 480 nm. A standard curve of doxorubicin concentration was prepared at concentrations of 0, 1, 2, 4, 6, 8, and 10 μg/mL and measured at 480 nm using Microplate Spectrophotometer. Subsequently, the Entrapment Efficiency (EE) and Loading Efficiency (LE) of O-CS-DOX NDs were calculated with blank O-CS NDs as the control, and the drug concentration of O-CS-DOX NDs was

calculated based on the above standard curve. All procedures were performed with protection of tinfoil to avoid the photodegradation of doxorubicin. EE and LE were calculated as follows: $EE = (A - B)/A \times 100\%$, $LE = (A - B)/(A + C) \times 100\%$, where A is the initial amount of doxorubicin in the solution, B is the amount of free doxorubicin in nanodroplets suspension, and C is the total amount of O-CS.

In vitro drug release study of O-CS-DOX NDs

EE and LE of O-CS-DOX NDs at different pH were evaluated before the drug release study of doxorubicin-loaded nanodroplets. O-CS-DOX NDs were immersed into phosphate buffer (pH 7.4) or acid buffer (pH 6.3) for 2 h at 4 ℃. At predetermined time intervals, the supernatants recovered from ultra-centrifuging of O-CS-DOX NDs solution were decanted. EE and LE were measured by the same method mentioned above.

The release of doxorubicin from O-CS-DOX NDs was performed using dialysis method (Meng et al. 2019). Briefly, 2 mL of the nanodroplets solution was placed in a dialysis membrane (MW cutoff 12,000 g/mol, Sigma) and immersed into 20 mL of phosphate buffer (pH 7.4) or acid buffer (pH 6.3). The release study was performed in a shaker incubator (Innova 40 Benchtop, Biocompare, USA) with shaking rate of 110 rpm at 37 ℃ for several days. At predetermined time intervals, the sampling was withdrawn and replaced with an equivalent volume of fresh buffer. The amount of released doxorubicin was measured by a Microplate Spectrophotometer at a wavelength of 480 nm. The accumulated release was calculated utilizing the equation (Meng et al. 2019).

To investigate the influence of ultrasound irradiation on doxorubicin release from O-CS-DOX NDs, the nanodroplets solution was sonicated by ultrasound (WED-100 ultrasonic therapy equipment, Honda Hi-Tech, China) for 0.5, 1, 2, 4, 8 and 10 min with different intensity (1.0 W/cm^2 in US1 group and 1.5 W/cm^2 in US2 group) at 37 ℃. After processing for predetermined time intervals, 1 mL of the nanodroplets solution was withdrawn and ultra-centrifuged. Then the free doxorubicin concentration in the supernatant was determined as described above.

Animals

All animal care and experimental protocols complied with the Animal Management Rules of Ministry of Health of People's Republic of China (document No 55, 2001). Animals on standard diet were maintained in a pathogen-free animal facility with a 12 h light–dark cycle. Six-to-eight-weeks-old healthy male nude mice were adopted by Pengyue Laboratory Animal Breeding Company (Shandong, China) and used to create PC-3 prostate tumor-bearing mouse model, followed by contrast-enhanced ultrasound imaging and therapeutic experiments. PC-3 cells (1×10^6 cells/mL) were harvested in exponential growth phase and were injected subcutaneously into the left or right forelimb of the mice. The length and width of tumors were measured using digital caliper and the tumor volume was calculated every other day. Mice were selected for experiments when their tumor volume reached 80 mm^3.

Ultrasound imaging of O-CS-DOX NDs in vitro and in vivo

In vitro ultrasound imaging experiments as in our previous study (Meng et al. 2019) were performed to investigate the ultrasonic imaging ability of O-CS-DOX NDs.

1.5 mL of nanodroplets solution at different concentrations (1.5×10^6–4.0×10^6/mL) were added to the plastic dropper fixed on the iron platform in water bath at 37 ℃. A clinical ultrasound scanner system (LOGIQ E9; GE, USA) was used with the major parameters (center frequency, 9.0 MHz; mechanical index, 0.5; focal length, 3.0 cm; dynamic range, 60 dB).

In the in vivo ultrasound imaging experiments of tumor-bearing mice, the clinical ultrasound scanner system mentioned above was also used with the major parameters (center frequency, 9.0 MHz; mechanical index, 0.22; focal length, 3.0 cm; dynamic range, 60 dB). Six tumor-bearing mice were randomly divided into O-CS-DOX NDs group and control group. 100 μL O-CS-DOX NDs suspensions or 100 μL PBS were administrated into the PC-3 tumor-bearing mice through tail vein injection when the sizes of subcutaneous tumor reached above 80 mm^3. After smearing the thick layer of couplant on the skin of the subcutaneous tumor, the two-dimensional, color doppler and contrast-enhanced ultrasound imaging were all performed.

Simultaneously, the average imaging intensity of each sample was detected using Image J software to analyze the gray-scale value. Circular regions of interest (ROIs) were outlined in each sample well. All experiments were conducted in triplicate.

Biosafety assessment of O-CS-DOX NDs in vivo

Healthy female mice were randomly divided into O-CS-DOX NDs-1 group, O-CS-DOX NDs-2 group and control group ($n = 10$ in each group). The mice in O-CS-DOX NDs-1 and -2 group were treated with 150 μL and 300 μL O-CS-DOX NDs respectively, while the mice in control group were injected with 300 μL saline intravenously. The general situations of the mice in each group were observed. The weight of mice was recorded on day 0, the 7th day and 14th day. Blood samples of all the mice were drawn on the 14th day for routine blood cell analysis and biochemical assays. All the mice were sacrificed to collect the major organs (heart, lung, kidney, and liver) for toxicity evaluation. The organ slices were stained with H&E staining after fixing with 4% paraformaldehyde for 24 h and observed using an optical microscope.

In vivo targeting capability and biodistribution of O-CS-DOX NDs

To evaluate the biodistribution of O-CS-DOX NDs, PC-3 tumor-bearing mice were randomly divided into four groups ($n = 5$ in each group): control group, O-CS-DOX NDs group, CS-DOX NDs group, and DOX group. The corresponding mice were intravenously administered 100 μL saline, 100 μL O-CS-DOX NDs, 100 μL CS-DOX NDs and the same dose of DOX. The tumor areas were immediately subjected to ultrasonic irradiation for 1 min after injection (output power density of 1.5 W/cm^2) in the O-CS-DOX NDs group and CS-DOX NDs group. The mice of each group were then anesthetized and placed into small animal imaging systems (IVIS Spectrum, PE, USA). All the procedures were carried out under light hindered conditions. The mice were imaged before administration and at different post administration time points (0, 2, 4, 8, 24 h). Quantitative analysis of the tumor regions was performed with Living Image software.

Anti-tumor effect of O-CS-DOX NDs in vivo

Thirty PC-3 tumor-bearing mice were randomly divided into six groups ($n = 5$ per group), including control group, DOX group, DOX + US group, O-CS-DOX NDs group, O-CS-DOX NDs + US group, CS-DOX NDs + US group. When the subcutaneous tumor volume reached approximately 80 mm^3, the mice were administered three systemic intravenous injections of various preparations (PBS, DOX, O-CS-DOX NDs and CS-DOX NDs) by tail vein on day 3, day 7 and day 11 with the same doxorubicin dose of 5 mg/kg, respectively. For the mice in the US group, tumor areas were immediately exposed to ultrasonic irradiation with coupling pad for 1 min after injection (output power density of 1.5 W/cm^2). The general situations of the mice in each group were observed. The body weight and tumor volume of the mice were measured every other day after the first treatment. A vernier caliper was used to measure the tumor volume at preset time. The tumor volume (V) was calculated by the following formula, where L is the major axis and D is the minor axis.

$$V = L \times D^2/2$$

The mice were sacrificed at day 14, tumors and major organs were removed. The tumor growth inhibition rate (TGI) was calculated by the formula: $TGI = (1 - V_t/V_0) \times 100\%$, where V_t is the tumor volume of experimental group and V_0 is the tumor volume of control group. Histopathological analysis was performed on the dissected tumors. The Ki-67 antigen staining and the terminal deoxynucleotidyl transferase-mediated dUTP nick end labeling (TUNEL) assay were performed according to the instructions of the kit. Apoptotic pictures were observed by fluorescence microscopy.

Statistical analysis

All the experiments were repeated at least three times. All data were expressed as the mean value with standard deviation (mean ± SD). The data were statistically analyzed with SPSS software (version 18.0; SPSS Inc, Chicago, IL, USA) using Student's t-test or one-way ANOVA analysis. $p < 0.05$ was considered statistically significant. All statistical tests were two tailed.

Results

Characterization of O-CS-DOX NDs

O-CS-DOX NDs solution appears an orange-red milky liquid. The SEM and TEM images of nanodroplets are reported in Fig. 1a, b, which showed that O-CS-DOX NDs had a spherical morphology with a well-defined core–shell structure. The light and fluorescence microscopic images of O-CS-DOX NDs (Fig. 1c, d) also showed discrete and spherical outlines, the latter of which was red because of the doxorubicin presence. Figure 1e, f showed that the typical mean diameter of O-CS-DOX NDs was (159.6 ± 24.2) nm with a narrow dispersion (PDI = 0.200 ± 0.021) and the zeta potential was (−8.42 ± 1.01) mV. The Entrapment Efficiency (EE) and Loading Efficiency (LE) of O-CS-DOX NDs were (93.37 ± 2.46) % and (50.07 ± 3.34) % at an optimal doxorubicin concentration of 1.5 mg/mL.

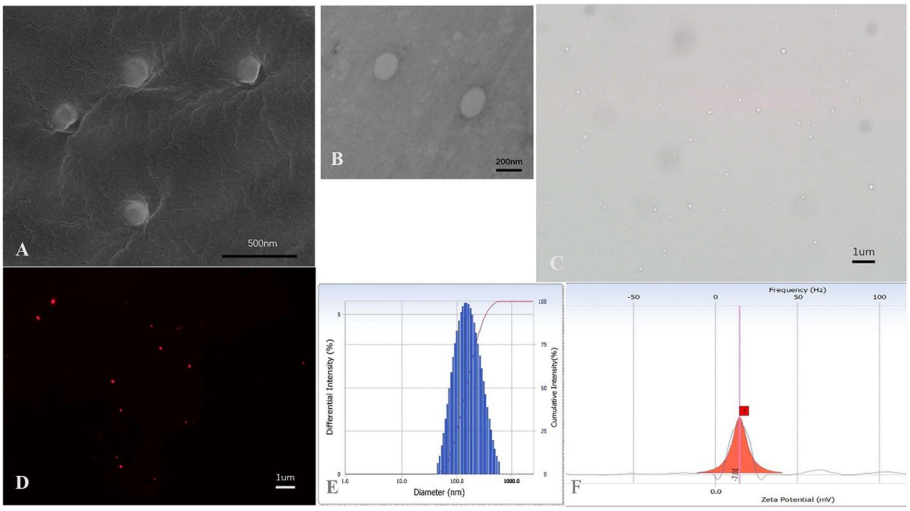

Fig. 1 Characteristics of O-CS-DOX NDs. **a, b** SEM and TEM images of O-CS-DOX NDs. **c, d** Light and fluorescence microscopic images of O-CS-DOX NDs. **e, f** The size distribution and zeta potential of O-CS-DOX NDs

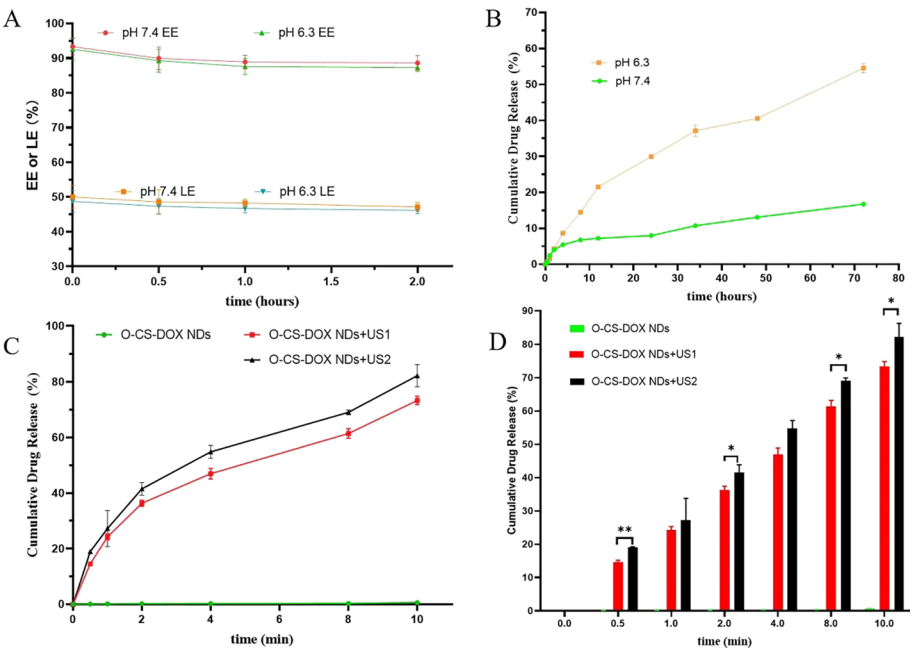

Fig. 2 Drug release study of O-CS-DOX NDs in vitro. **a** The influences of pH values on the encapsulation efficiency (EE) and loading efficiency (LE) of O-CS-DOX NDs within 2 h. **b** Doxorubicin release from O-CS-DOX NDs in pH 7.4 and 6.3 at 37 ℃ for 72 h. **c, d** Release of doxorubicin from O-CS-DOX NDs without ultrasound (control) and with ultrasound exposure at pH 7.4, at 37 ℃ for 10 min. The intensity of O-CS-DOX NDs + US1 group is 1.0 W/cm^2 and that of O-CS-DOX NDs + US2 group is 1.5 W/cm^2, asterisks (*) denote significant differences (*$p < 0.05$, **$p < 0.01$)

Drug release study of O-CS-DOX NDs in vitro

As illustrated in Fig. 2a, EE and LE of O-CS-DOX NDs had slightly but no obvious changes at both pH 7.4 and 6.3 in 2 h. The in vitro drug release profile of doxorubicin

from O-CS-DOX NDs at different pH is exhibited in Fig. 2b and the drug-loaded nanodroplets showed a sustained and pH-dependent profile. 54.5% of doxorubicin was release from the nanodroplets after 72 h at pH 6.3, while only 16.7% was released at pH 7.4. The effect of ultrasound irradiation on the drug release of O-CS-DOX NDs was also evaluated. The cumulative amount of doxorubicin released was only 0.63% in 10 min without ultrasound irradiation. Under ultrasound exposure (1.0 W/cm^2 in US1 group and 1.5 W/cm^2 in US2 group) at 37 ℃ for 10 min, massive amount (73.3% in US1 group and 82.3% in US2 group) of doxorubicin released from the nanodroplets (Fig. 2c, d) with obvious significant difference between US1 and US2 group ($p < 0.05$).

Ultrasound imaging of O-CS-DOX NDs in vitro and in vivo

Ultrasound imaging experiments illustrated in our previous study (Meng et al. 2019) (Fig. 3a) were carried out in water bath at 37 ℃ to study the ultrasonic imaging ability of O-CS-DOX NDs in vitro, using a clinical ultrasound scanner (LOGIQ E9; GE, USA) system. As can be seen from Fig. 3b, c O-CS-DOX NDs showed satisfactory ultrasound enhancement ability which was dose-dependent. The contrast enhancement ultrasound imaging intensity of O-CS-DOX NDs became significantly stronger as the concentration of nanodroplets increased ($p < 0.05$). The PBS group did not have any ultrasonic imaging signals under the same experimental conditions.

The ultrasound imaging capability of O-CS-DOX NDs in vivo was further explored. The B-mode, color doppler mode and contrast enhanced mode images of ultrasound were all collected before and after the tail veil injection of the nanodroplets. As shown in Fig. 4a, the subcutaneous tumor of the mice appeared hypoechoic solid nodule without necrosis in B-mode imaging and the volume of tumor in O-CS-DOX NDs group and control group were 119.76 ± 10.03 mm^3 and 131.08 ± 9.73 mm^3, respectively. Color doppler flow imaging showed tiny blood flow through the tumors. It is worth noting that

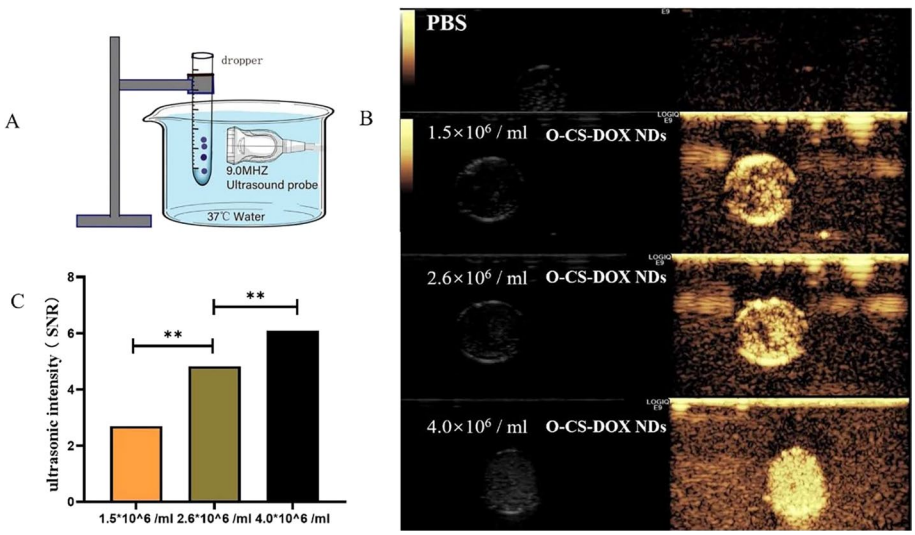

Fig. 3 Ultrasound enhancement imaging ability of O-CS-DOX NDs in vitro. **a** Schematic illustration of the in vitro imaging experimental setup; **b** ULtrasound contrast enhanced images of various concentrations of O-CS-DOX NDs. **c** Comparison of the contrast imaging abilities (signal to noise ratio, SNR) between various concentrations of O-CS-DOX NDs, asterisks (*) denote significant differences (**$p < 0.01$)

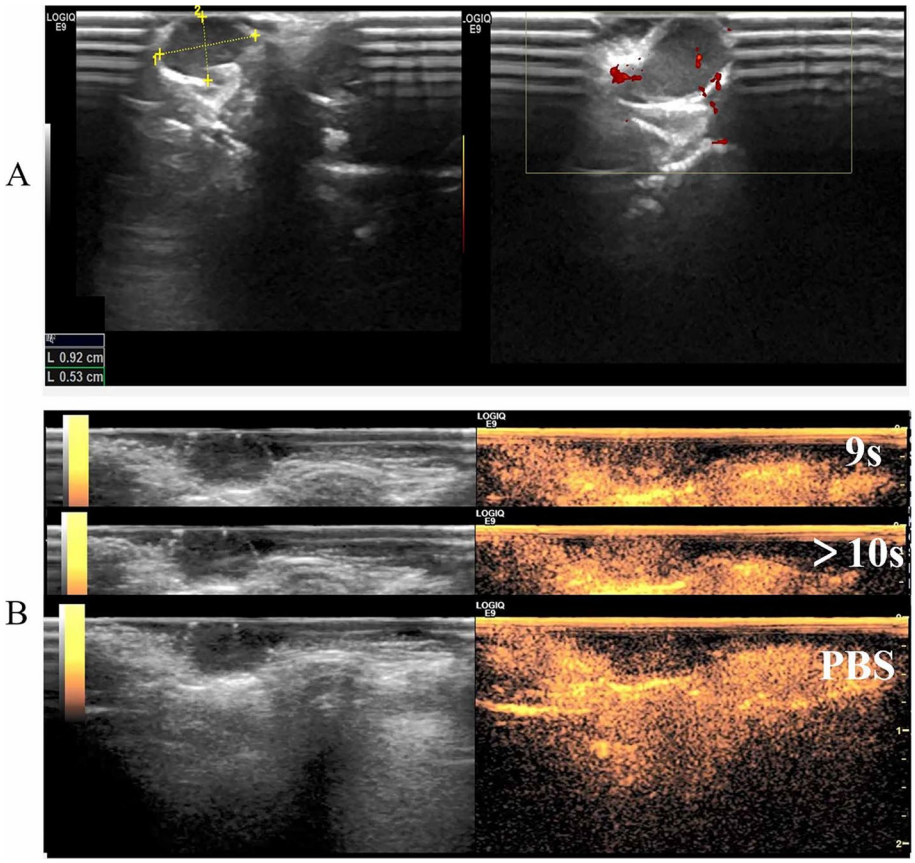

Fig. 4 Ultrasound enhancement imaging ability of O-CS-DOX NDs in vivo. **a** In vivo ultrasound and CDFI imaging ability of O-CS-DOX NDs; **b** In vivo ultrasound enhancement imaging ability of O-CS-DOX NDs 9 s group, O-CS-DOX NDs 10-60 s group and PBS group

Table 1 body weight in different groups of nude mice at different times (g)

Group	0 day	7 days	14 days
Control	22.5 ± 0.41	23.3 ± 0.61	24.1 ± 0.49
O-CS-DOX NDs-1	23.0 ± 0.70	24.1 ± 0.85	24.8 ± 1.18
O-CS-DOX NDs-2	23.3 ± 0.44	23.5 ± 1.01	23.8 ± 1.14

weak contrast enhanced ultrasound imaging signals were observed after 9 s of injection (Fig. 4b). And the intensity was gradually enhanced in 1 min and weakened after that. In contrast, there was no significant difference in the contrast-enhanced ultrasound images of the tumor sites of control group.

Biosafety evaluation of O-CS-DOX NDs in vivo

O-CS-DOX NDs (150 μL or 300 μL) or 300 μL saline were intravenously injected via the tail vein to assess the safety of drug-loaded nanodroplets. During the 2-week period after administration, two mice showed lethargy and another two mice showed temporary instability on the first day, all of which returned to normal soon. There was no significant

Table 2 Blood routine parameters of nude mice after 14 days

Parameters	Control	O-CS-DOX NDs-1	O-CS-DOX NDs-2
WBC ($\times 10^9$)	3.77 ± 0.21	3.72 ± 0.18	3.84 ± 0.08
RBC ($\times 10^9$)	9.83 ± 0.05	9.89 ± 0.08	9.74 ± 0.11
MONO ($\times 10^9$)	2.47 ± 0.19	2.69 ± 0.25	2.22 ± 0.08
LYMPH ($\times 10^9$)	0.27 ± 0.03	0.36 ± 0.07	0.35 ± 0.02
HGB (g/L)	138.67 ± 4.04	139.33 ± 10.26	141.33 ± 3.21
PLT ($\times 10^{12}$)	1032.33 ± 3.79	1100 ± 71.55	1073 ± 37.75
NEURO ($\times 10^9$)	1.05 ± 0.15	1.0 ± 0.10	0.96 ± 0.23

Table 3 Blood biochemical parameters of nude mice after 14 days

Parameters	Control	O-CS-DOX NDs-1	O-CS-DOX NDs-2
ALT (U/L)	69.67 ± 15.14	79.00 ± 12.49	80.33 ± 9.02
AST (U/L)	119.33 ± 13.61	142.33 ± 27.15	105.33 ± 7.57
BUN (mmol/L)	8.63 ± 0.61	8.70 ± 0.26	6.50 ± 1.05
CRE (umol/L)	21.00 ± 2.65	24.67 ± 3.21	21.33 ± 4.16
ALB (g/L)	26.90 ± 1.28	28.17 ± 1.00	29.37 ± 1.86
LDH (U/L)	569.00 ± 57.51	740.33 ± 74.97	680 ± 102.78

difference in body weight and serum parameters between these three groups (Tables 1, 2, 3). Histological examination of the main organs showed no significant lesions in the heart, liver, lung and kidney, and the structural integrity of the cells of these organs were maintained without cellular edema and shrinkage (Fig. 5).

In vivo fluorescence imaging of tumor-bearing mice

To investigate the tumor accumulation ability, the local fluorescence intensity of mice in different groups were observed using IVIS imaging system at 0, 2, 4, 8 and 24 h after intravenously injection of PBS, equivalent DOX, O-CS-DOX NDs, and CS-DOX NDs. The DOX, O-CS-DOX NDs, and CS-DOX NDs all generated high fluorescent signals in tumor regions immediately after administration. Moreover, the strong fluorescence of doxorubicin in the tumors of mice remained 24 h after injection in the O-CS-DOX NDs and CS-DOX NDs group (Fig. 6a). Comparing with that, the fluorescence intensity of the tumors in the DOX group decreased gradually, which was weak after 24 h. The results in Fig. 6b showed that the average fluorescence intensity of the tumors in the O-CS-DOX NDs group was stronger than that in the CS-DOX NDs group and DOX group with significant differences ($p < 0.01$).

Antitumor efficacy of O-CS-DOX NDs in vivo

PC-3 tumor-bearing mice were used to evaluate the in vivo tumor growth inhibition for the therapeutic assessment of O-CS-DOX NDs combined with ultrasound irradiation. Various formulations including PBS, DOX, O-CS-DOX NDs, and CS-DOX NDs were given to mice by intravenous injection via the tail vein with or without ultrasound irradiation on preset day (days 3, 7, 11) once the tumor volume reached approximately 80 mm^3. During the therapeutic period, the tumor volumes and body weight of mice

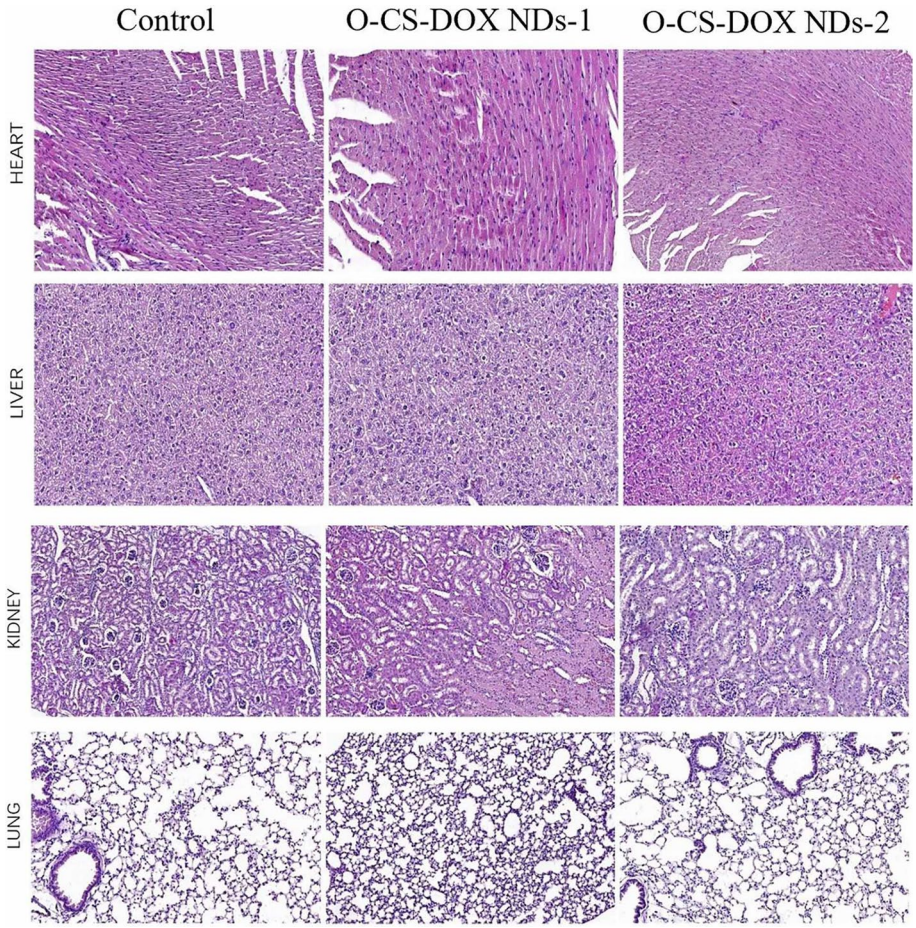

Fig. 5 Light microscopic of HE staining of heart, liver, kidney and lung in nude mice after application of O-CS-DOX NDs in vivo

were monitored every other day. The subcutaneous tumors were photographed after the mice were sacrificed on day 14, which are shown in Fig. 7a. The results in Fig. 7a, b and Table 4 show that the tumor volume of mice in different groups was in the following order: PBS > O-CS-DOX NDs > DOX > DOX + US > CS-DOX NDs + US > O-CS-DOX NDs + US. Significant effects on tumor growth inhibition were seen in the nanodroplets or doxorubicin groups when compared to PBS group. Moreover, the O-CS-DOX NDs + US group exhibited the highest efficiency in inhibiting tumor growth and the treatment began to take effect after 8 days (the second day after the second administration). Tumors of O-CS-DOX NDs + US group were significantly smaller than those from O-CS-DOX NDs treated tumors, whereas DOX + US group did not exhibit statistical differences compared with the group treated with DOX. More interestingly, the O-CS-DOX NDs + US group exhibited much stronger inhibition of tumor growth compared to the CS-DOX NDs + US group. However, the group injected with O-CS-DOX NDs without ultrasound irradiation showed bigger tumors at the end of treatment. All the above results were further confirmed by the data of tumor growth inhibition rate in Fig. 7c. As shown in Fig. 7d and Table 5, doxorubicin solution in both DOX group and DOX + US group induced significant body weight reduction of the mice, while nanodroplets

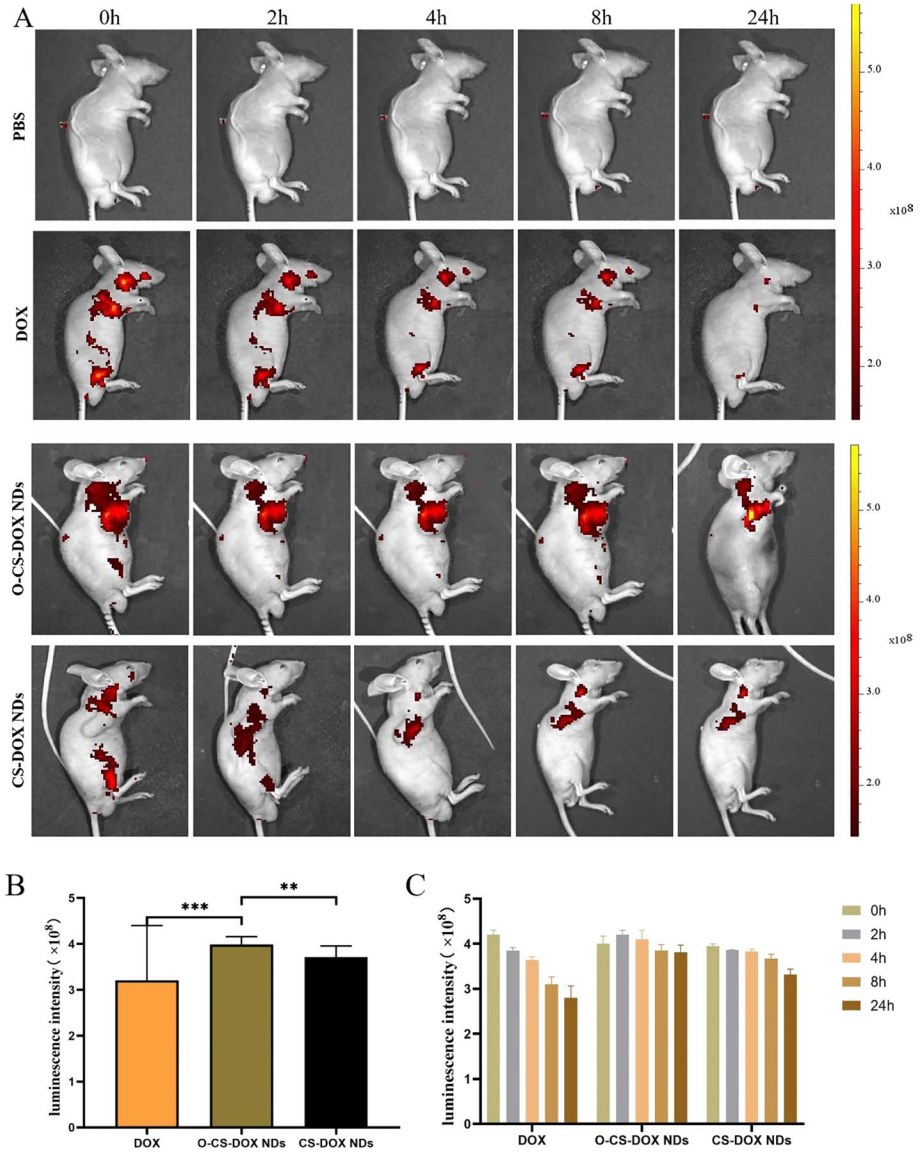

Fig. 6 In vivo fluorescence imaging of tumor-bearing mice. **a** In vivo imaging of mice in PBS, DOX, O-CS-DOX NDs and CS-DOX NDs group at different time points ($n = 5$). **b** Comparison of average luminescence intensity of tumors-bearing mice between different groups during the experiment. **c** The luminescence intensity of tumors-bearing mice at the certain time between different groups during the experiments. Asterisks (*) denote significant differences (**$p < 0.01$, ***$p < 0.001$)

formulations in other groups did not exhibit significant loss of weight throughout the period of experiments.

After the various treatments, the antitumor effect was further assessed by pathological analysis of the tumor. H&E staining was used to examine the histological features of the tumor induced by different formulations. As seen in Fig. 8a, tumor sections from the PBS and O-CS-DOX NDs group were densely cellular and presented nuclear polymorphism. What's more, the tumor tissues in the other four groups were dramatically damaged which presented in obvious chromatic agglutination, karyopyknosis, or nuclear fragmentation of the target tumor cells. Among which, the fewest tumor

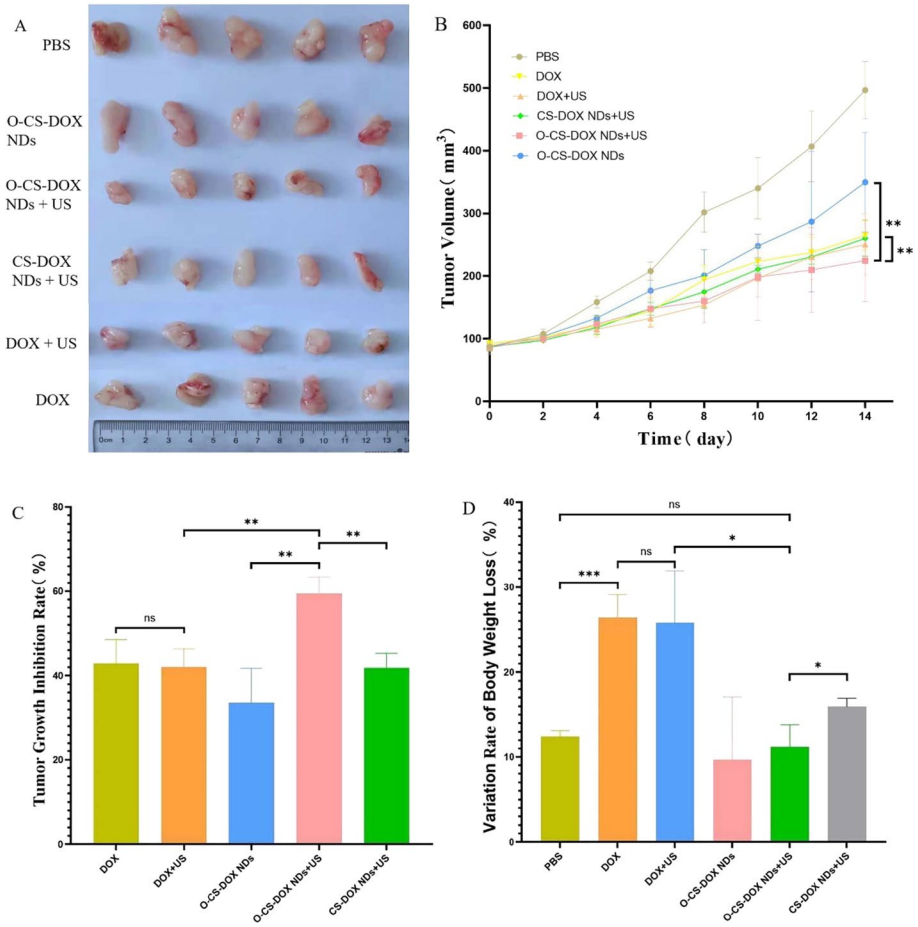

Fig. 7 In vivo antitumor effect. **a** Photographs of PC-3 tumor tissues collected from six groups at the end of treatment ($n=5$). **b** Tumor volumes of mice in six groups during the therapeutic period. **c** Tumor growth inhibition rates in each group according to the tumor volumes. **d** Body weights loss of mice at the end of treatment. Asterisks (*) denote significant differences (*$p<0.05$, **$p<0.01$), and ns means no significant differences ($p>0.05$)

Table 4 Tumor volumes at different times of mice in different groups (mm^3)

Group	0 day	2 days	4 days	6 days	8 days	10 days	12 days	14 days
PBS	87.10 ± 12.2	107.9 ± 7.83	158.7 ± 9.69	208.1 ± 14.8	302.0 ± 32.0	340.2 ± 48.7	406.8 ± 56.2	496.7 ± 45.9
DOX	92.2 ± 5.27	103.0 ± 4.92	121.1 ± 15.4	144.0 ± 21.7	194.1 ± 23.0	223.4 ± 23.8	237.8 ± 24.3	264.8 ± 23.7
DOX + US	89.0 ± 8.27	103.9 ± 10.9	114.9 ± 12.6	132.6 ± 13.7	153.7 ± 13.4	196.7 ± 29.7	230.4 ± 35.9	250.7 ± 48.5
O-CS-DOX NDs	86.9 ± 6.08	101.4 ± 9.18	133.0 ± 4.80	176.8 ± 30.6	200.9 ± 41.5	247.9 ± 18.8	312.0 ± 90.7	349.8 ± 79.5
O-CS-DOX NDs + US	86.1 ± 5.02	100 ± 3.73	123.3 ± 11.3	147.9 ± 29.7	160.2 ± 34.6	198.4 ± 68.9	209.8 ± 67.4	224.7 ± 65.3
CS-DOX NDs + US	86.8 ± 6.08	99.5 ± 3.03	118.0 ± 10.8	147.9 ± 9.97	174.8 ± 26.5	211.0 ± 6.34	230.7 ± 11.7	260.2 ± 28.4

cells and largest necrosis were observed in the O-CS-DOX NDs + US group. In addition, immunohistochemistry (the Ki-67 antigen staining and TUNEL assay) was performed to assess the tumor cell proliferation and apoptosis in situ. Figure 8b, c shows that the tumor tissues of the mice treated with O-CS-DOX NDs + US complexes

Table 5 Body weight at different times of mice in different groups (g)

Group	0 day	2 days	4 days	6 days	8 days	10 days	12 days	14 days
PBS	19.48 ± 3.14	19.19 ± 2.64	19.11 ± 2.66	18.40 ± 2.35	18.56 ± 2.37	18.06 ± 2.33	17.85 ± 2.62	17.74 ± 2.65
DOX	16.78 ± 2.33	16.60 ± 2.43	16.40 ± 2.40	16.12 ± 2.57	16.14 ± 3.01	15.50 ± 2.78	14.33 ± 3.38	13.53 ± 3.17
DOX + US	18.51 ± 2.76	18.21 ± 2.73	17.99 ± 2.84	17.85 ± 2.94	17.58 ± 3.30	16.38 ± 2.52	15.01 ± 2.68	14.17 ± 3.10
O-CS-DOX NDs	18.28 ± 2.09	18.05 ± 2.08	18.00 ± 2.21	17.68 ± 2.15	17.95 ± 2.79	17.50 ± 2.54	16.76 ± 3.15	16.22 ± 3.22
O-CS-DOX NDs + US	17.17 ± 3.52	16.85 ± 4.04	16.75 ± 3.92	16.32 ± 3.83	15.82 ± 3.72	15.51 ± 3.66	14.98 ± 3.44	14.65 ± 3.52
CS-DOX NDs + US	16.98 ± 2.24	16.57 ± 2.08	16.72 ± 2.34	16.22 ± 2.12	15.69 ± 1.6	15.34 ± 1.85	14.77 ± 1.35	13.93 ± 1.53

showed the lowest level of Ki-67 positive cells and the highest level of cell apoptosis compared to the other treated cases. The immunohistochemical data were all consistent with the in vivo antitumor efficacy.

Discussion

In the present study, we assessed the features and performances of the prepared pH-dependent charge-conversion nanodroplets about tumor imaging and treatment on animal experiments with another manufacturing method. The promising advantages of this system were maintained in PC-3 tumor-bearing mice, which were (a) ideal nanoscale size and negative zeta potential; (b) good doxorubicin loading ability and pH-sensitive and ultrasound-responsive drug release; (c) excellent ultrasound imaging ability; (d) good safety and biocompatibility; (e) great tumor accumulation and enhanced antitumor effect in vivo.

The unique doxorubicin-loaded nanodroplets (O-CS-DOX NDs) were constructed through an improved mild nano-emulsion method using ultrasonic emulsification instead of mechanical oscillation used in our previous study. The size of O-CS-DOX NDs was (159.6 ± 24.2) nm with a narrow dispersion, which was smaller than that of nanodroplets manufactured by mechanical homogenizer we used before. What's more, the concentration of nanodroplets increased and more droplets were found under the light microscope. One possible reason is that, ultrasonic cavitation effect of ultrasonic emulsification may play a more important role in the formation of more and smaller nanodroplets in addition to high shear force. These new fabricated nanodroplets were still found to have well-defined spherical morphology with a core/shell structure and appeared as discrete red dots in the fluorescence microscope because of the successful loading of doxorubicin. A key feature of O-CS-DOX NDs is negative-to-positive charge conversion under an acidic environment, which was confirmed by measuring the change in surface charge of nanodroplets in our previous study (Meng et al. 2019). EE and LE of doxorubicin in O-CS-DOX NDs here was (93.37 ± 2.46) % and (50.07 ± 3.34) %, which were both higher than those of nanodroplets prepared in our previous study. The advantage of ultrasonic emulsification over mechanical oscillation on developing nanoparticles still need to be further studied.

The drug release experiments were carried out again because of its importance in the drug delivery system. The results showed that doxorubicin released very slowly at pH 7.4 and exhibited an accelerated drug release profile in acidic media (pH 6.3),

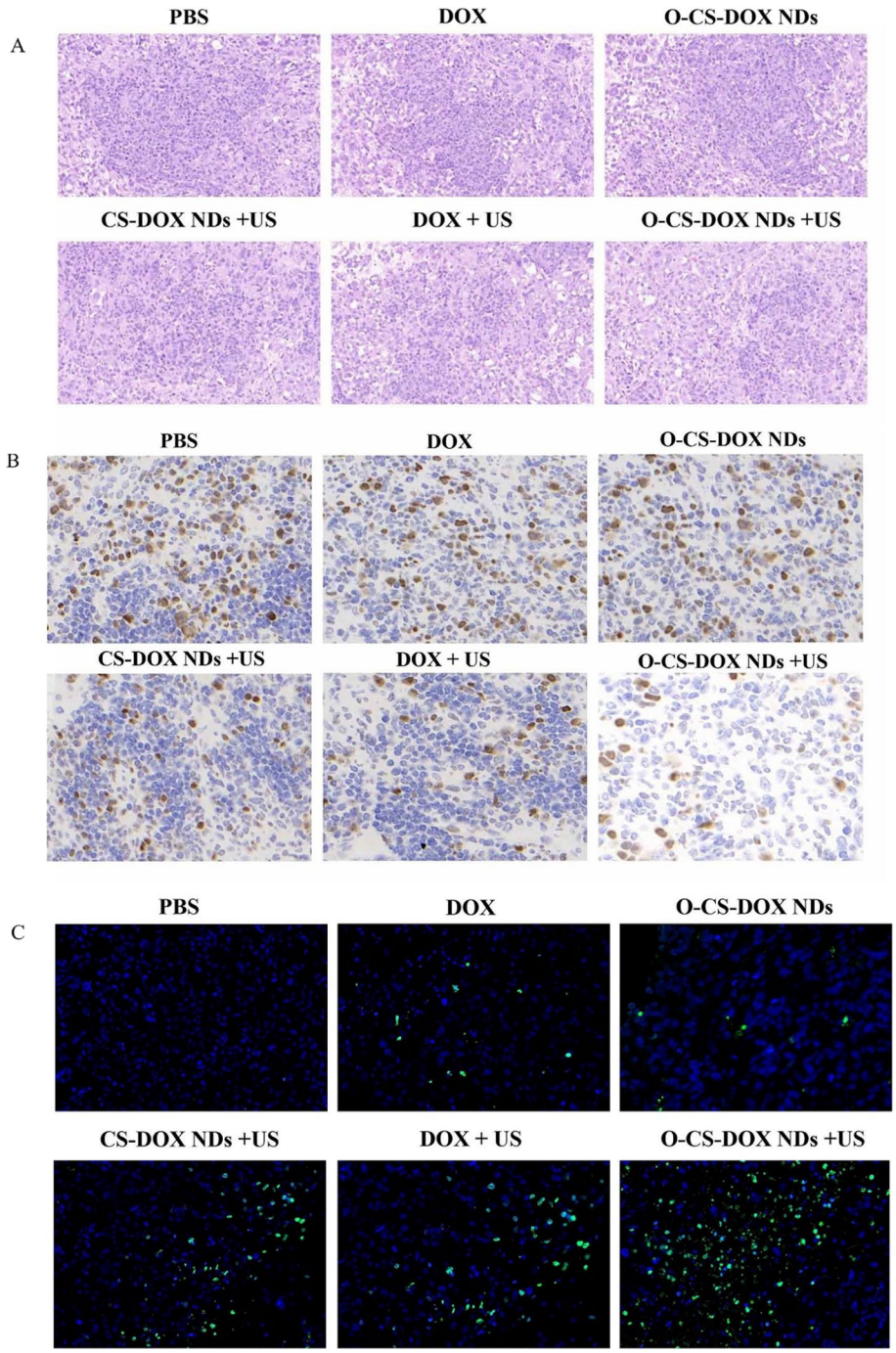

Fig. 8 Pathological analysis and immunohistochemistry of tumor tissues in different groups. **a** H&E staining of tumor tissues after treatment in different groups. **b** Ki67 positive tumor cells after treatment in different groups. **c** TUNEL positive tumor cells after treatment in different groups

indicating the pH-sensitive drug release mode of these nanodroplets as previously studied. The better solubility of doxorubicin in subacid environment, the protonation-induced deformation of O-CS in the surface of O-CS-DOX NDs and the subsequent larger size of O-CS-DOX NDs were inferred to lead to the rapid drug release at

lower pH. The ultrasound-aided drug release study confirmed that ultrasound exposure could trigger the rapidly burst release of doxorubicin from O-CS-DOX NDs after ultrasound irradiation for 10 min. The acoustic droplet vaporization (ADV) and bubble formation under the action of ultrasound could involve the drug-release process. What's more, the cumulative release ratio increased as the intensity of ultrasonic irradiation enhanced with significance difference. Therefore, the higher power (1.5 W/cm^2) of ultrasonic therapy was used in subsequent experiments.

The doxorubicin-loaded nanodroplets in our study were superior to common drug-loaded nanoparticles because they could be used for ultrasound-responsive imaging. It can be found from Fig. 3b that O-CS-DOX NDs still showed good contrast-enhanced ultrasound imaging ability. In addition, the brightness of contrast-enhanced ultrasonic signals was increasing, as the concentration of nanodroplets increased from 1.5×10^6/mL to 4.0×10^6/mL. The dose-dependent echo intensities in the region of interest are also calculated in Fig. 3c and were consistent with the ultrasound imaging findings. We further explored the ultrasound imaging capability of O-CS-DOX NDs in vivo. It is worth noting that contrast-enhanced ultrasound imaging signals were observed after 9 s of injection and the signal intensity was significantly enhanced within 1 min (Fig. 4), which indicated that sufficient O-CS-DOX NDs accumulated in the targeted tumor sites rapidly and underwent a phase change. The peak time of contrast-enhanced ultrasound signal was faster than that in the previous studies of various ultrasound-responsive nanoparticles (Mou et al. 2019; Guo et al. 2020; Gao et al. 2021), which may due to the proper size, high stability in blood circulation and pH-sensitive features of O-CS-DOX NDs and the specialty of PC-3 prostate tumor. Thus, the nanodroplets here present great potential for use in ultrasound-induced tumor-targeting imaging and treatment.

Based on the high physical stability, hemocompatibility and low cytotoxicity demonstrated in our previous work (Meng et al. 2019) and Additional file 1: Fig. S1, the in vivo toxicity assays were analyzed to further evaluate the biocompatibility and biosafety of O-CS-DOX NDs, which are the prerequisites to ensure their subsequent clinical application. Considering that doxorubicin-loaded nanodroplets may cause undesired side effects, such as weight loss, hematotoxicity and organ toxicity, the body weight of mice was recorded every one week and the blood was collected for blood cell analysis and biochemical examination two weeks after intravenous injection. The results of Table 1 show that no significant body weight loss was observed in the groups of O-CS-DOX NDs. As shown in Table 2, there was no significant difference in the parameters of blood cell among all the groups, suggesting no syndrome was elicited, such as hemolytic anemia or acute infection. In addition, there were no meaningful changes in indicators of hepatotoxicity and nephrotoxicity (Table 3). The histological analysis of main organs (heart, liver, lung, and kidney) indicated that no obvious abnormal damage (degeneration or necrosis) in all the O-CS-DOX NDs groups and PBS group (Fig. 5). Therefore, all the results discussed above suggested O-CS-DOX NDs would be a promising candidate for effective and safe doxorubicin delivery in cancer therapy.

To observe the in vivo biodistribution and accumulation of nanodroplets in tumor tissue, the fluorescence signal was acquired by the IVIS Spectrum imaging system at varied time points and the average luminescence intensity of all the groups were calculated. As depicted in Fig. 6a, the tumor regions of the O-CS-DOX NDs and free doxorubicin

groups were all highlighted with a fluorescence signal immediately after injection, indicating the rapid delivery to tumor sites. During the time after administration, the free doxorubicin displayed weaker and weaker fluorescence signal as the passage of time and the signal almost disappeared at 24 h after injection, which showed the instability and rapid clearance of naked drug in vivo. In contrast, the tumor sites of O-CS-DOX NDs groups kept highlighted with strong fluorescence signal the whole time, demonstrating the in vivo stability, successful delivery and continuously accumulating in the tumor regions of O-CS-DOX NDs. Interestingly, the fluorescence signal of CS-DOX NDs was not detected until two hours post injection and was relatively weaker all the time, which suggested that fewer nanodroplets were delivered slowly to the targeted tumor tissues. And the average fluorescence intensities in the CS-DOX NDs group were significantly lower than that in the O-CS-DOX NDs group (Fig. 6b). These results, coinciding with conclusions obtained by our previous study in vitro (Meng et al. 2019), suggested that O-CS-DOX NDs were more qualified as a promising drug delivery system than CS-DOX NDs in vivo.

Another attractive feature of our nanodroplets was the enhanced anti-cancer ability under ultrasound stimulation in vivo. According to digital photographs and tumor growth curves (Fig. 7a–c; Table 4), tumors of O-CS-DOX NDs + US group were smallest, and the O-CS-DOX NDs + US group exhibited the highest efficiency in inhibiting tumor growth, with the inhibition taking effect one day after the second administration (day 8). Tumors of O-CS-DOX NDs + US group were significantly smaller than those from O-CS-DOX NDs treated tumors, whereas DOX + US group did not exhibit statistical differences compared with the group treated with DOX. These results indicated that ultrasound irradiation was prerequisite and played a key role in nanodroplets mediated therapy. What's more, The O-CS-DOX NDs + US group exhibited much stronger inhibition of tumor growth compared to the CS-DOX NDs + US group, further indicating the more superior anti-tumor effectiveness of O-CS-DOX NDs in vivo than that of CS-DOX NDs, which were in good consistent with the results above discussed. Besides, the group injected with O-CS-DOX NDs without ultrasound irradiation showed bigger tumors at the end of treatment, suggesting that the good drug retaining of nanodroplets and potentially guarantee the in vivo biosafety of O-CS-DOX NDs. The body weight of the mice decreased continuously during the whole period of experiment among all the groups (Fig. 7d; Table 5). No significant body weight loss was observed in the groups of nanodroplets formulations, while doxorubicin solution in both DOX group and DOX + US group induced significant body weight reduction of the mice, indicating the high biosafety and low toxicity of O-CS-DOX NDs application in vivo. The therapeutic efficacies of various groups were further compared through pathological analysis, the Ki-67 antigen staining and TUNEL assay (Fig. 8). Consistent with the antitumor efficacy studies, the tumor tissues of the mice treated with O-CS-DOX NDs and ultrasound irradiation showed the lowest level of Ki-67 positive cells, suggesting that tumor cell proliferation was strongly decreased by this treatment. Meanwhile, in this same group the highest level of cell apoptosis was detected, indicating that this combination therapy was much more effective in inducing apoptosis of tumor cells. The mechanical and thermal effects of ultrasound irradiation may also take part in damaging the tumor tissues and tumor cells apoptosis. Based on the aforementioned in vivo therapeutic results, we

concluded that the combination of O-CS-DOX NDs and ultrasound irradiation could exert a formidable therapeutic effect against PC-3 prostate cancer.

The O-CS-DOX NDs in this study showed promising in terms of in vivo stability, ultrasound echogenicity, biocompatibility, and enhanced anticancer effect with the aid of ultrasound irradiation. The results of this study confirmed that O-CS-DOX NDs were more superior to CS-DOX NDs. Still further investigation in vivo will be needed to explore the feasibility of this nanoplatform as a multi stimulus-responsive targeted theranostic agent for tumor detection and for image-guided chemotherapy.

Conclusion

In this study, we assessed the in vivo application of smart O-carboxymethyl chitosan/PFH doxorubicin-loaded nanosized delivery system. These multi stimulus-responsive O-CS-DOX NDs have several advantages in animal studies. Firstly, nanodroplets with small size (< 200 nm) and good doxorubicin encapsuling ability could be detected through conventional ultrasound with satisfying contrast-enhanced imaging ability. Secondly, the great biocompatibility and biosafety of these nanodroplets guarantee the application in vivo. Thirdly, these nanodroplets had high stability and effectively accumulated in the targeted tumor tissues, which ensure the sufficient drug concentration solely in the tumor sites. Finally, and most importantly, this nanodroplets combined with ultrasound irradiation could enhance the killing effects on tumors. This research of the advantages of O-CS-DOX NDs application in vivo showed the promising potential as a smart multi-responsive bomb to effectively diagnosis and kill cancer cells.

Supplementary Information

The online version contains supplementary material available at https://doi.org/10.1186/s12645-023-00172-z.

Additional file 1: Figure S1 (A) In vitro biocompatibility of O-CS-DOX NDs at varied concentrations for 24 h treatment. (B) In vitro biocompatibility of O-CS-DOX NDs at varied concentrations for 48 h treatment.

Acknowledgements
This work was supported by National Natural Science Foundation of China (Nos. 82071937, 81771843).

Author contributions
Dong Meng, Lu Guo, and Jie Li had designed the experiment. Dong Meng, Shan Xiao, Yading Zhao, and Xiaoxuan Wang had conducted the experiment. Xiao Sun, Dandan Shi, Xiaoying Zhou, and Mengmeng Shang had contributed to the study on the materials and instruments. Dong Meng wrote the manuscript. Lu Guo and Jie Li had reviewed the manuscript. All authors read and approved the final manuscript.

Funding
This work was supported by National Natural Science Foundation of China (Nos. 82071937, 81771843).

Availability of data and materials
The raw data supporting the conclusions of this article will be made available by the authors, without undue reservation. All data generated during this study are included in this article.

Declarations

Ethics approval and consent to participate
All animal studies in our research were in compliance with licensed procedures approved by the Institutional Animal Care of Qilu Hospital of Shandong University (No. KYLL-2021(KS)-900).

Consent for publication
Not applicable.

Competing interests
The authors declare no competing interests.

Received: 11 May 2022 Accepted: 5 March 2023
Published online: 11 March 2023

References

Bae YH, Park K (2011) Targeted drug delivery to tumors: myths, reality and possibility. J Control Release 153:198–205
Chang S, Si T, Zhang S, Merrick MA, Cohn DE, Xu RX (2016) ULtrasound mediated destruction of multifunctional microbubbles for image guided delivery of oxygen and drugs. Ultrason Sonochem 28:31–38
Chen EM, Quijano AR, Seo YE, Jackson C, Josowitz AD, Noorbakhsh S et al (2018) Biodegradable PEG-poly(ω-pentadecalactone-co-p-dioxanone) nanoparticles for enhanced and sustained drug delivery to treat brain tumors. Biomaterials 178:193–203
Chong WK, Papadopoulou V, Dayton PA (2018) Imaging with ultrasound contrast agents: current status and future. Abdominal Radiol (New York) 43:762–772
Denison TA, Bae YH (2012) Tumor heterogeneity and its implication for drug delivery. J Control Release 164:187–191
Fisher R, Pusztai L, Swanton C (2013) Cancer heterogeneity: implications for targeted therapeutics. Br J Cancer 108:479–485
Gao X, Guo D, Mao X, Shan X, He X, Yu C (2021) Perfluoropentane-filled chitosan poly-acrylic acid nanobubbles with high stability for long-term ultrasound imaging in vivo. Nanoscale 13:5333–5343
Golombek SK, May JN, Theek B, Appold L, Drude N, Kiessling F et al (2018) Tumor targeting via EPR: strategies to enhance patient responses. Adv Drug Deliv Rev 130:17–38
Guo H, Xu M, Cao Z, Li W, Chen L, Xie X et al (2020) ULtrasound-assisted miR-122-loaded polymeric nanodroplets for hepatocellular carcinoma gene therapy. Mol Pharm 17:541–553
Han Y, Pan J, Liang N, Gong X, Sun S (2021) A pH-sensitive polymeric micellar system based on chitosan derivative for efficient delivery of paclitaxel. Int J Mol Sci 22:6659
Kanamala M, Wilson WR, Yang M, Palmer BD, Wu Z (2016) Mechanisms and biomaterials in pH-responsive tumour targeted drug delivery: a review. Biomaterials 85:152–167
Kelly CM, Power DG, Lichtman SM (2014) Targeted therapy in older patients with solid tumors. J Clin Oncol 32:2635–2646
Lee J, Min HS, You DG, Kim K, Kwon IC, Rhim T et al (2016) Theranostic gas-generating nanoparticles for targeted ultrasound imaging and treatment of neuroblastoma. J Control Release 223:197–206
Li Y, Yang J, Xu B, Gao F, Wang W, Liu W (2015) Enhanced therapeutic siRNA to tumor cells by a pH-sensitive agmatine–chitosan bioconjugate. ACS Appl Mater Interfaces 7:8114–8124
Liu J, Huang Y, Kumar A, Tan A, Jin S, Mozhi A et al (2014a) pH-sensitive nano-systems for drug delivery in cancer therapy. Biotechnol Adv 32:693–710
Liu F, Li M, Liu C, Liu Y, Zhang N (2014b) PH-sensitive self-assembled carboxymethyl chitosan-modified DNA/polyethylenimine complexes for efficient gene delivery. J Biomed Nanotechnol 10:3397–3406
Long M, Liu S, Shan X, Mao J, Yang F, Wu X et al (2020) Self-assembly of pH-sensitive micelles for enhanced delivery of doxorubicin to melanoma cells. J Drug Deliv Sci Technol 59:101859
Ma X, Yao M, Shi J, Li X, Gao Y, Luo Q et al (2020) High intensity focused ULtrasound-responsive and ULtrastable cerasomal perfluorocarbon nanodroplets for alleviating tumor multidrug resistance and epithelial-mesenchymal transition. ACS Nano 14:15904–15918
Markman JL, Rekechenetskiy A, Holler E, Ljubimova JY (2013) Nanomedicine therapeutic approaches to overcome cancer drug resistance. Adv Drug Deliv Rev 65:1866–1879
Meng D, Guo L, Shi D, Sun X, Shang M, Zhou X et al (2019) Charge-conversion and ultrasound-responsive O-carboxymethyl chitosan nanodroplets for controlled drug delivery. Nanomedicine (Lond) 14:2549–2565
Mou C, Yang Y, Bai Y, Yuan P, Wang Y, Zhang L (2019) Hyaluronic acid and polydopamine functionalized phase change nanoparticles for ultrasound imaging-guided photothermal-chemotherapy. J Mater Chem B 7:1246–1257
Movahedi F, Hu RG, Becker DL, Xu C (2015) Stimuli-responsive liposomes for the delivery of nucleic acid therapeutics. Nanomed Nanotechnol Biol Med 11:1575–1584
Rosenblum D, Joshi N, Tao W, Karp JM, Peer D (2018) Progress and challenges towards targeted delivery of cancer therapeutics. Nat Commun 9:1410
Shen S, Li Y, Xiao Y, Zhao Z, Zhang C, Wang J et al (2018) Folate-conjugated nanobubbles selectively target and kill cancer cells via ultrasound-triggered intracellular explosion. Biomaterials 181:293–306
Shi J, Kantoff PW, Wooster R, Farokhzad OC (2017) Cancer nanomedicine: progress, challenges and opportunities. Nat Rev Cancer 17:20–37
Sonawane SJ, Kalhapure RS, Govender T (2017) Hydrazone linkages in pH responsive drug delivery systems. Eur J Pharmaceut Sci 99:45–65
Thakkar S, Sharma D, Kalia K, Tekade R. Tumor microenvironment targeted nanotherapeutics for cancer therapy and diagnosis: a review. Acta Biomater 2019;101.
Tian H, Guo Z, Lin L, Jiao Z, Chen J, Gao S et al (2014) pH-responsive zwitterionic copolypeptides as charge conversional shielding system for gene carriers. J Control Release 174:117–125
van der Meel R, Sulheim E, Shi Y, Kiessling F, Mulder WJM, Lammers T (2019) Smart cancer nanomedicine. Nat Nanotechnol 14:1007–1017
Wang L, Geng D, Su H (2014) Safe and efficient pH sensitive tumor targeting modified liposomes with minimal cytotoxicity. Colloids Surf B 123:395–402
Wang G, Wu B, Li Q, Chen S, Jin X, Liu Y et al (2020) Active transportation of liposome enhances tumor accumulation, penetration, and therapeutic efficacy. Small 16:e2004172
Wei P, Gangapurwala G, Pretzel D, Leiske MN, Wang L, Hoeppener S et al (2019) Smart pH-sensitive nanogels for controlled release in an acidic environment. Biomacromol 20:130–140

Yang G, Phua SZF, Lim WQ, Zhang R, Feng L, Liu G et al (2019) A hypoxia-responsive albumin-based nanosystem for deep tumor penetration and excellent therapeutic efficacy. Adv Mater (Deerfield Beach, FLA) 31:e1901513
Yao Y, Su Z, Liang Y, Zhang N (2015) pH-Sensitive carboxymethyl chitosan-modified cationic liposomes for sorafenib and siRNA co-delivery. Int J Nanomed 10:6185–6197
Yusa S (2017) Stimuli-responsive polymer micelles. In: Kawai T, Hashizume M (eds) Stimuli-responsive interfaces. Springer, Singapore. https://doi.org/10.1007/978-981-10-2463-4_11
Zhao H, Xu J, Wan J, Geng S, Li H, Peng X et al (2017) Cisplatin-directed coordination-crosslinking nanogels with thermo/pH-sensitive triblock polymers: improvement on chemotherapic efficacy via sustained release and drug retention. Nanoscale 9:5859–5871

Publisher's Note